

Evidence of strong short-range order in $(\text{Fe}_{0.2}\text{Co}_{0.8})_{75}\text{Si}_x\text{B}_{25-x}$ amorphous alloys from EXAFS spectroscopy

M. L. Fdez-Gubieda, I. Orúe, F. Plazaola, and J. M. Barandiarán

Departamento Electricidad y Electrónica, Facultad de Ciencias, Universidad del País Vasco, Apartado Postal 644, 48080 Bilbao, Spain

(Received 13 February 1995; revised manuscript received 6 July 1995)

Liquid-quenched metallic amorphous alloys $(\text{FeCo})_{75}\text{SiB}$ were prepared with the aim of studying the influence of the relative metalloid concentration over the short-range order in these alloys. Room-temperature x-ray-absorption spectra have been recorded on the Fe and Co K edge at the Daresbury Laboratory. Both the extended x-ray-absorption fine structure (EXAFS) and x-ray-absorption near-edge structure (XANES) spectra present clear evidence of a very different chemical and topological short-range order around the Fe and Co atom in all the studied samples. The XANES region suggests the existence of a strong chemical short-range order characterized by a preferential coordination of B with Fe and Si with Co. This assumption has been proven by the EXAFS study. Moreover, the gradual appearance of a shoulder at around 4 \AA^{-1} when the Si content increases, in the Fe K -edge EXAFS spectra, has been proven to be evidence of the existence of a very ordered structure involving higher-order coordination shells than the first one.

I. INTRODUCTION

The Fe-Co-based amorphous alloys have been the subject of several investigations with different experimental techniques due to their interesting magnetic properties.¹ In particular, the Fe-Co-Si-B amorphous alloys have good soft magnetic properties combined with high saturation polarization, crystallization temperatures, and Curie temperatures over wide composition ranges.² The introduction of Co into Fe-B systems increases the magnetic polarization J_s , and the addition of Si raises the crystallization temperature of these amorphous alloys. Moreover, these alloys present positive saturation magnetostrictions in the Fe-rich side and negative ones in the Co-rich end.^{3,4} A particular dependence on alloy composition has been found for the induced magnetic anisotropy^{5,6} and the magnetostriction.⁷ These results support the existence of a short-range order (SRO) with different structural units over different ranges of sample composition.⁸ Besides, a close relationship between stress-induced anisotropy and viscoelastic deformation parameters⁹ or resistivity changes,¹⁰ has been interpreted as arising from changes of the chemical short-range order as a function of composition.

Extended x-ray-absorption fine structure (EXAFS) studies¹¹ in $(\text{Fe}_x\text{Co}_{1-x})_{75}\text{Si}_{15}\text{B}_{10}$ metallic glasses provide strong evidence of different chemical and topological environments of the Fe and Co atoms as well as the existence of a more ordered structure around Fe for $x \approx 0.2$. A nonhomogeneous distribution of metalloids with a preferential coordination of Fe with B and Co with Si was suggested as the main cause of the strong SRO changes observed in the Co-rich side of the alloys. However, in that work¹¹ the EXAFS analysis was performed assuming a Gaussian radial distribution function, causing the average distances and coordination numbers to shift to smaller values.

Very recently, Mössbauer spectroscopy¹² has been performed in $(\text{Fe}_y\text{Co}_{1-y})_{75}\text{Si}_x\text{B}_{25-x}$ with the aim of studying separately the influence of the metals Fe and Co and the metalloids Si and B on the isomer shift (IS) and the magnetic

hyperfine field (B_{hf}) which are strongly related to both the SRO and bonding properties involving Fe atoms. The dependence of the hyperfine parameters on x and y was shown to be very different for the Fe-rich side ($y > 0.5$) than for the Co-rich one ($y < 0.5$). In the case of samples corresponding to $y < 0.5$, the large changes observed in the hyperfine parameters as a function of both x and y were related to strong SRO changes in this range of composition. Specifically, it was found that the SRO increases with both the Co and Si content. It has been suggested that some quite defined structural units exist in such range of Fe/Co concentrations.

In the present work, we have used x-ray-absorption spectroscopy, both EXAFS and x-ray absorption near-edge structure (XANES), to obtain a deeper knowledge about the SRO dependence on the Si/B relative concentration in $(\text{Fe-Co})_{75}\text{Si-B}$ alloys. Thus we have chosen a series of samples of composition $(\text{Fe}_{0.2}\text{Co}_{0.8})_{75}\text{Si}_x\text{B}_{25-x}$ corresponding to the Co-rich side of the system Fe-Co-Si-B with different Si/B relative concentrations x equal to 0%, 5%, 10%, and 15%. We present the experimental details in Sec. II, the data analysis in Sec. III, the XANES and EXAFS results in Sec. IV, and the discussion of both x-ray-absorption results in Sec. V. In Sec. VI we briefly outline the main conclusions.

II. EXPERIMENT

All the samples were obtained by the standard single-roller quenching technique¹³ in the form of long ribbons with typical cross sections 0.5 mm wide and 20 μm thick. The amorphous nature of the ribbons so obtained has been checked by x-ray diffraction and magnetic measurements.

The room-temperature x-ray-absorption spectra on the Fe and Co K edge were recorded in the 7.1 station at the Daresbury Synchrotron Radiation Source using a Si(111) monochromator and 50% of harmonic rejection in the usual transmission geometry. The storage ring was running with an electron energy of 2 GeV and a current between 120 and 250 mA.

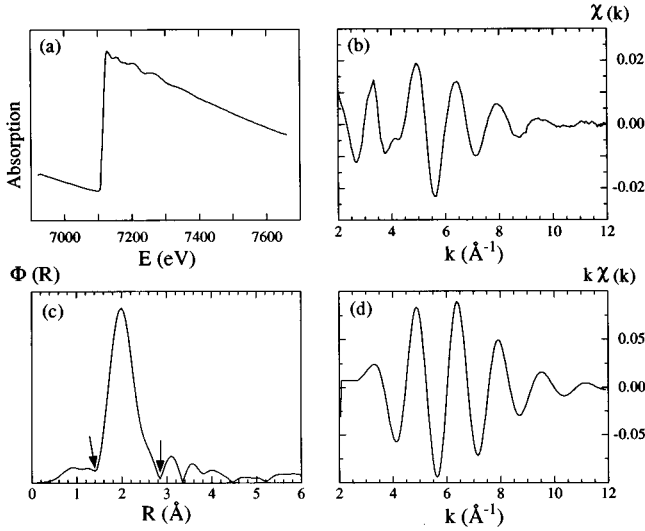


FIG. 1. (a) Typical x-ray-absorption spectrum. (b) Raw EXAFS spectrum $\chi(k)$. (c) Fourier transform $\Phi(R)$ of $\chi(k)$. (d) Inverse Fourier transform of $\Phi(R)$, $k\chi^F(k)$, in the range marked by the arrows in (c).

III. DATA ANALYSIS

The normalized EXAFS functions $\chi(k)$ [Fig. 1(b)] have been extracted from the raw data [Fig. 1(a)] using a standard procedure.¹⁴ The appearance of the Co *K* edge at around 700 eV above the Fe *K* edge limits the *k* range for the EXAFS oscillations in Fe up to 12 \AA^{-1} . Thus the absorption above the edge [see Fig. 1(a)] has been fitted using a three cubic spline in the *k* range $2 \leq k \leq 14 \text{\AA}^{-1}$ for the Co edge and in $2 \leq k \leq 12 \text{\AA}^{-1}$ for the Fe edge. Figures 2(a) and 3(a) show the Co and Fe *K*-edge spectra $\chi(k)$ of $(\text{Fe}_{0.2}\text{Co}_{0.8})_{75}\text{Si}_x\text{B}_{25-x}$ for $x=0, 5, 10$, and 15, with a low noise level obtained in all of them. The origin of the *k* space has been taken at the inflection point of the absorption edge. In all the cases, the Fourier transform of $\chi(k)$, $\Phi(R)$ [see Fig. 1(c)], performed in the *k* range $2 \leq k \leq 12 \text{\AA}^{-1}$ with a k^3 weight and a Hanning window function, yields a broad peak well isolated at the apparent position of 2 \AA [see Figs. 2(b) and 3(b)]. The inverse transform of $\Phi(R)$ in the region of the main peak allows us to obtain a filtered $k\chi^F(k)$ signal in *k* space [see Fig. 1(d)] which can be used to simulate the structure of the first coordination shell around Fe and Co in these glasses.

In the analysis of amorphous samples, a general approach in terms of the partial radial distribution function (RDF) $g_j(r)$ should be used, where the EXAFS function is given by

$$k\chi(k) = \sum_j f_j(k, \pi) e^{-2\sigma_j^2 k^2} \int \frac{e^{-2\Gamma_j/k}}{r^2} \times g_j(r) \sin[2kr + \phi_j(k)] dr, \quad (1)$$

$f_j(k, \pi)$ being the backscattering amplitude function of atoms of type *j* around the absorbing atom. ϕ_j is the total phase shift, $e^{-2\Gamma_j/k}$ is a mean free path term that takes into account the inelastic losses, and σ_j is the Debye-Waller factor. *k* is the wave vector of the photoelectron, which is related to the electron mass (*m*) and the threshold energy (E_0) by

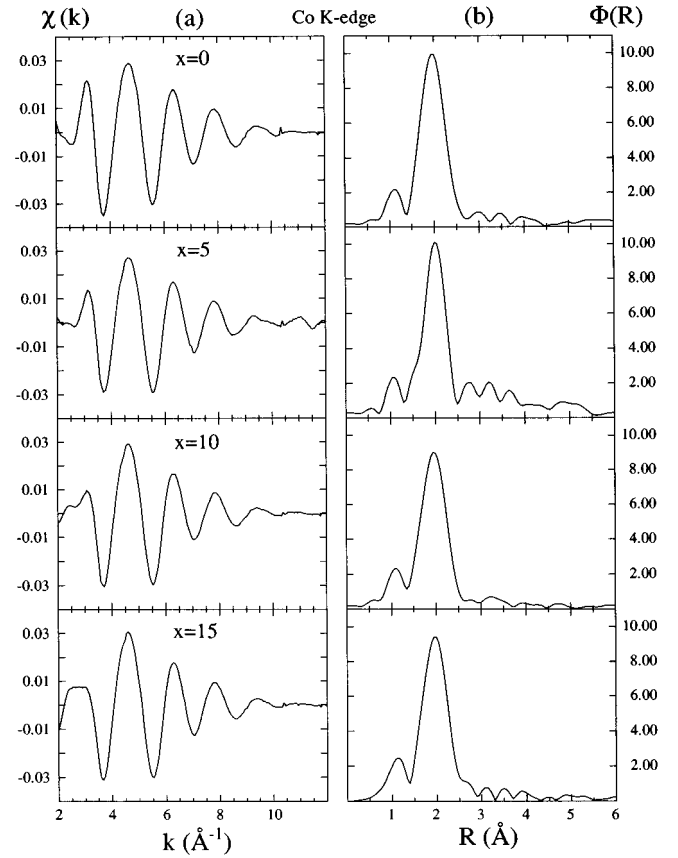


FIG. 2. (a) EXAFS spectra of the Co *K* edge corresponding to $(\text{Fe}_{0.2}\text{Co}_{0.8})_{75}\text{Si}_x\text{B}_{25-x}$ for $x=0, 5, 10$, and 15. (b) Fourier transform $\Phi(R)$ corresponding to spectra in (a).

$$k = \left[\frac{2m}{\hbar^2} (E - E_0) \right]^{1/2}. \quad (2)$$

A Gaussian RDF, although working very well with harmonic crystals, has been proved inadequate for disordered systems.¹⁵ The use of a Gaussian RDF gives rise to a first shell distance displaced to smaller *r* values than the actual interatomic distances obtained by x-ray and scattering measurements. This difference between EXAFS and x-ray diffraction (XRD) results is attributed to the occurrence of a very asymmetrical nearest-neighbor distribution.^{15,16} In this work we have used the following RDF, proposed by De Crescenzi *et al.*¹⁷ in the framework of the dense random packing of hard spheres (DRPHS) model:

$$g_j(r) = \begin{cases} \frac{1}{\sigma_{D_j}} e^{-(r-R_j)/\sigma_{D_j}} & \text{for } r \geq R_j, \\ 0 & \text{for } r < R_j, \end{cases} \quad (3)$$

where R_j becomes the distance between the centers of the two touching spheres, *j*, and σ_{D_j} is the root-mean-square deviation of distances between *j* atoms and the absorbing atom. The average distance will then be given by $\hat{R}_j = R_j + \sigma_{D_j}$. By introducing this $g_j(r)$ in Eq. (1), one can obtain the following expression for $k\chi(k)$:^{15,17}

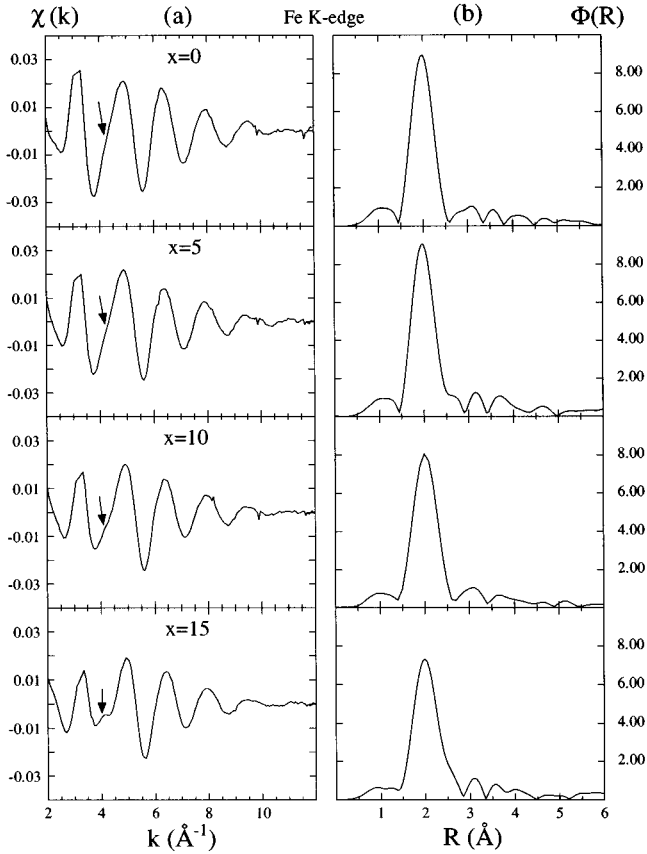


FIG. 3. (a) EXAFS spectra of the Fe K edge corresponding to $(\text{Fe}_{0.2}\text{Co}_{0.8})_{75}\text{Si}_x\text{B}_{25-x}$ for $x=0, 5, 10,$ and 15 . The gradual appearance of a shoulder is observed (marked with an arrow) at around 4 \AA^{-1} . (b) Fourier transform $\Phi(R)$ corresponding to spectra in (a).

$$k\chi(k) = \sum_j N_j f_j(k, \pi) \frac{e^{-2\sigma_j^2 k^2} e^{-2\Gamma_j/k}}{R_j^2} \frac{1}{\sqrt{1+4k^2\sigma_{D_j}^2}} \times \sin[2kR_j + \tan^{-1}(2k\sigma_{D_j}) + \phi_j], \quad (4)$$

where the sum extends in our case over the four species of backscattering atoms (Fe, Co, Si, and B). N_j is the number of atoms of j type around the absorbing atom. This expression has already been proved to give good results in other metallic glasses like $\text{Fe}_{80}\text{B}_{20}$,¹⁷ $\text{Co}_{80}\text{P}_{20}$,¹⁸ and $\text{Ni}_{80}\text{P}_{20}$,¹⁸ with good agreement between the EXAFS and XRD results. However, EXAFS spectroscopy is able to give more detailed results than XRD techniques since it is more sensitive to the nearest distance R_j than to average distance \hat{R}_j .

In order to get structural information, i.e., coordination numbers and distances of the atoms surrounding a given one, it is necessary to introduce in Eq. (4) the backscattering amplitudes and phase shifts of the pairs involved, obtained from calculations or experimental models. In our case such backscattering parameters have been taken from the FEFF3 codes.¹⁹ Using the backscattering parameters from the calculations of McKale *et al.*,²⁰ very similar results to the ones obtained in this study have been found²¹ in the Co K edge of $(\text{Fe}_{0.2}\text{Co}_{0.8})_{75}\text{Si}_x\text{B}_{25-x}$.

The optimization of scattering factors has been performed using as reference compounds fcc Co, CoSi_2 , bcc Fe, Fe_2B ,

TABLE I. Summary of EXAFS results on films and powder standards: coordination numbers N , interatomic distance R , and Debye-Waller factor σ (f , film standard; p , powder standards; F , fix from crystallographic data (Ref. 22); *, the spectrum was obtained at liquid nitrogen temperature). XRD data from Ref. 22.

Sample	N	EXAFS R (\AA)	σ^2 (\AA^2)	XRD R (\AA)
bcc Fe^f	8.3 (7) (Fe)	2.472 (5)	0.004 (4)	2.482
	5.5 (6) (Fe)	2.852 (4)	0.005 (4)	2.866
Fe_2B^p	4^F (B)	2.126 (5)	0.0009(4)	2.184
	1^F (Fe)	2.399 (3)	0.000 (3)	2.383
	2^F (Fe)	2.471 (4)	0.0067(4)	2.455
	4^F (Fe)	2.668 (5)	0.0049(4)	2.699
	4^F (Fe)	2.713 (5)	0.0020(4)	2.712
Fe_3Si^p	5.3^F (Fe)	2.447 (4)	0.006 (4)	2.447
	4^F (Fe)	2.802 (4)	0.011 (4)	2.825
	2.7^F (Si)	2.447 (3)	0.006 (3)	2.447
	2^F (Si)	2.802 (3)	0.012 (4)	2.825
fcc Co^f	12 (7) (Co)	2.492 (5)	0.002 (4)	2.50
CoSi_2^p	12^F (Co)	3.811 (4)	0.007 (4)	3.794
	8^F (Si)	2.308 (4)	0.005 (4)	2.323

and Fe_3Si . The results from these standards are presented in Table I. The interatomic distance values obtained from the EXAFS analysis are in good agreement with those taken from the XRD data.²²

The theoretical expression (4) becomes extremely complicated for the case of alloys with four different backscattering atoms, as in our case (Fe, Co, Si, and B). However, some restrictions can be taken into account that simplify the fitting process. One can assume that Fe and Co behave almost identically as backscatterers. This is so because the backscattering amplitudes and phase shifts are very similar for Fe and Co atoms (see Fig. 4 for backscattering amplitudes). Thus, in the following, the contribution of both transition-metal atoms to the Fe and Co K -edge EXAFS spectra will be considered as coming from the same backscattering atom, named M . In this way, the theoretical EXAFS function of the Co and Fe K

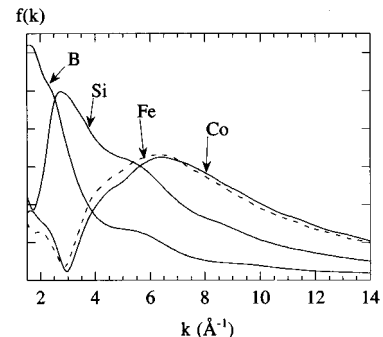


FIG. 4. Backscattering amplitudes (taken from FEFF3 codes) of atoms located at the following distances from the absorbing atom: Fe and Co at 2.5 \AA , B at 2 \AA , and Si at 2.25 \AA .

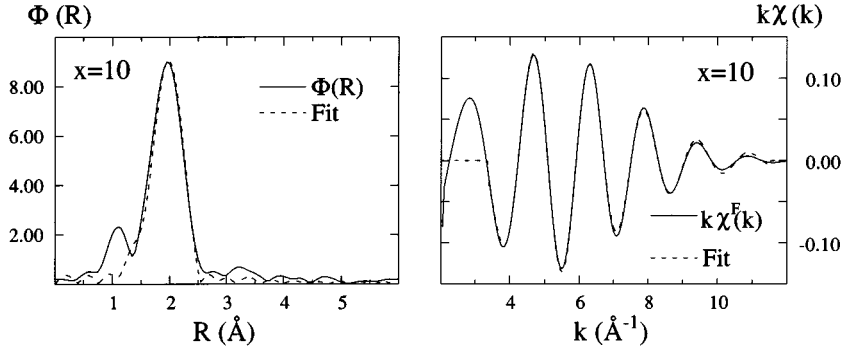


FIG. 5. Left, Fourier transform of raw EXAFS, $\Phi(R)$, with Fourier transform of the fit of $k\chi^F(k)$, and right, inverse Fourier transform $k\chi^F(k)$ plus the corresponding fit in the Co K edge of $x=10$.

edge becomes a linear combination of three individual EXAFS signals: the first one due to the M - M pairs (M =Fe, Co), the second one coming from the M -Si ones, and the third one from the M -B pairs. The Debye-Waller factors (σ_j), particular for each backscatterer, have been assumed to be equal for the four studied samples. No relevant change of structural parameters is obtained if σ_j is allowed to vary. The Γ_j parameter (which is related to the photoelectron mean free path) has been taken from the polycrystalline standards Fe_3Si and Fe_2B ($\Gamma_j=1 \text{ \AA}^{-1}$). These present a local structure that consists of multiple atomic shells very close to each other over the range 2–3 \AA (see Table I), more similar to the amorphous structure than the other standards. During the fitting procedure, the change in the threshold energy between the metal and metalloids (ΔE_0) was considered to be the same as that obtained in the reference compounds ($\Delta E_0 \approx 2 \text{ eV}$ for both metalloids Si and B). Anyway, as we shall discuss later, there are too many free parameters involved in Eq. (4) to face the fittings without other considerations.

Finally, the fitting procedure uses a least-squares algorithm to minimize the standard deviation, defined as

$$S = \frac{\sum_p (\chi_p^F - \chi_p)^2 k_p}{\sum_p (\chi_p^F)^2 k_p}, \quad (5)$$

where the sum extends over all the experimental points p corresponding to the wave vector k_p , χ_p^F , and χ_p are, respectively, the values of the Fourier-filtered experimental data and theoretical function of Eq. (4) corresponding to k_p . The obtained minima of S are between 1.4×10^{-2} and 6×10^{-4} for all the spectra. Figure 5 shows that the fits so obtained are rather satisfactory both in R space and k space. The error bar of each parameter has been obtained by changing that particular parameter until the contribution of the parameter to S is twice the starting one.²³

The XANES spectra have been obtained first by subtracting from the measured absorption coefficient μ a linear background extrapolated from below the edge. Then the curves have been normalized to the height of the absorption step at the edge.

IV. RESULTS

A. XANES results

Figure 4 shows that, in the XANES region (low- k range), the backscattering amplitudes of low atomic number, like Si or B, become greater than those of transition-metal atoms, like Fe or Co. Therefore, the XANES becomes much more

sensitive than the EXAFS to the location of metalloid atoms like the Si and B in the first coordination shell around the metal atoms (Fe and Co).²⁴

Figure 6 shows the XANES spectra of the Co and Fe K edges for the four amorphous alloys with different Si/B concentration. It becomes clear at a first glance that the Fe and Co XANES spectra become completely different when B is gradually substituted by Si. In the Co edge such substitution leads to a large change of the shape of XANES. A peak appears at around 20 eV above the absorption energy that greatly increases with increasing the Si content. The general shape of the Fe XANES spectra remains almost unchanged, i.e., very similar to that presented for the sample without Si, $x=0$. The very different behavior of the Fe and Co XANES spectra suggests a preferential location of the Si atom around the Co one. A similar result has been previously reported by Kizler²⁵ of a preferred occurrence of the Ni-P and Fe-B pairs in $\text{Fe}_{40}\text{Ni}_{40}\text{P}_{14}\text{B}_6$ amorphous alloys. The resemblance of the Ni edge XANES with that of the binary $T_{80}\text{P}_{20}$ alloys (T =Fe or Ni) and of the Fe edge XANES with the binary $T_{80}\text{B}_{20}$ supports the previous assertion. Taking into account the comparison with Kizler's results, Fig. 6 indicates a preferred occurrence of Co-Si and Fe-B pairs.

We must point out that a quantitative analysis of the XANES data requires the use of complex calculations involving multiple scattering effects.²⁶ Anyway, the qualitative analysis of XANES has allowed us to obtain very clear information about the chemical short-range order (CSRO) in our alloys. This preferential chemical atomic arrangement found from XANES has been taken into account in the quantitative analysis of the EXAFS data and so it can be thought of as a tool to simplify the initial complexity of our task.

B. EXAFS results

As commented previously, the EXAFS analysis of a quaternary alloy becomes very difficult due to the large number

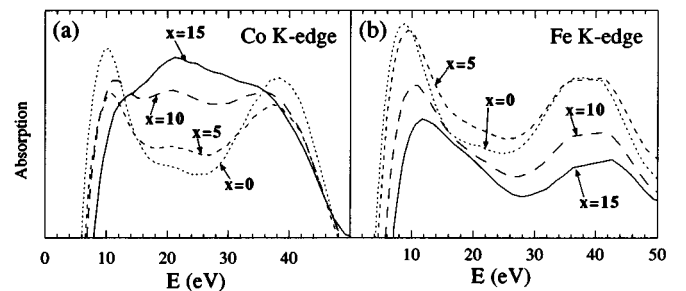


FIG. 6. XANES spectra of $(\text{Fe}_{0.2}\text{Co}_{0.8})_{75}\text{Si}_x\text{B}_{25-x}$ ($x=0, 5, 10$, and 15) at the (a) Co K edge and (b) Fe K edge.

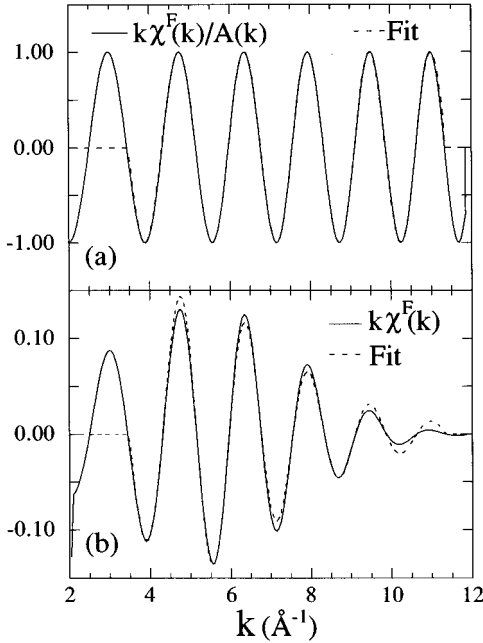


FIG. 7. (a) Inverse Fourier transform divided by its envelope function, $k\chi^F(k)/A(k)$, with the corresponding fit for the Co K edge of $x=0$. (b) Inverse Fourier transform $k\chi^F(k)$ plus the fit assuming only one Co- M contribution, with R and σ_D fixed from the fit in (a).

of free parameters involved in the fitting procedure. We have started the fitting process with the spectra corresponding to the simplest sample, the ternary amorphous alloy $(\text{Fe}_{0.2}\text{Co}_{0.8})_{75}\text{B}_{25}$ ($x=0$). Once reliable coordination numbers and interatomic distances have been achieved, the analysis has been extended to the samples with increasing Si content.

The B atom backscattering amplitude is much smaller than the M atom one for $k > 3 \text{ \AA}^{-1}$ (see Fig. 4). This fact together with the small relative concentration of B in the alloy should allow one to consider the B contribution negligible. If this approximation is reliable, the Fe and Co EXAFS of $x=0$ should fit to only one EXAFS signal, coming from the M - M interference. Therefore, the phase of the experimental inverse Fourier transform deduced by dividing $k\chi^F(k)$ by its envelope function $A(k)[k\chi^F(k)/A(k)]$ should fit very well with a single sine function.²⁷

$$\sin[2kR + \tan^{-1}(2k\sigma_D) + \phi(k)]. \quad (6)$$

TABLE II. Values of structural parameters relative to the neighborhood of Co atoms for $(\text{Fe}_{0.2}\text{Co}_{0.8})_{75}\text{Si}_x\text{B}_{25-x}$ amorphous samples: coordination numbers N , nearest interatomic distance R , mean deviation of interatomic distance, σ_D , and average interatomic distance $\hat{R} = R + \sigma_D$.

Sample	S	Co- M				N	Co-B			Co-Si			
		N	R (Å)	σ_D (Å)	\hat{R} (Å)		N	R (Å)	σ_D (Å)	\hat{R} (Å)	N	R (Å)	σ_D (Å)
$x=0$	1.39×10^{-2}	12 (1)	2.360 (2)	0.23 (3)	2.59 (3)								
	4.14×10^{-3}	11.3 (9)	2.372 (5)	0.21 (2)	2.58 (2)	1.1 (6)	2.06 (6)	0.00 (1)	2.06 (7)				
	4.89×10^{-3}	12 (1)	2.373 (5)	0.26 (2)	2.63 (3)								
$x=5$	6.17×10^{-4}	11.2 (4)	2.384 (3)	0.25 (1)	2.63 (1)	0.8 (4)	2.04 (3)	0.00 (3)	2.04 (6)				
	4.26×10^{-3}	11.1 (9)	2.389 (7)	0.27 (2)	2.66 (3)					1 (1)	2.23 (3)	0.00 (2)	2.23 (5)
$x=15$	5.69×10^{-3}	11 (1)	2.392 (8)	0.26 (2)	2.65 (3)					1.1 (9)	2.25 (4)	0.00 (3)	2.25 (7)

This method allows one to avoid the correlation between the amplitude and the phase of $k\chi(k)$ due to the presence of the term σ_D in both [see Eq. (4)].

1. Co K edge

Following the previous approximation, Eq. (6) fits rather well the phase of the EXAFS function $[k\chi^F(k)/A(k)]$ corresponding to the sample with $x=0$ [see Fig. 7(a)]. This clearly indicates that the approximations made during the fitting are correct: Fe and Co can be considered as the same backscatterer, and the B contribution in this sample is negligible. The values of the nearest-neighbor distance ($R_{\text{Co-M}}$) and mean deviation ($\sigma_{D_{\text{Co-M}}}$) so obtained have been used to fit [see Fig. 7(b)] the total EXAFS function, which now depends only on the coordination number of M around Co ($N_{\text{Co-M}}$), and Debye-Waller factor $\sigma_{\text{Co-M}}$.

If we do not neglect the boron contribution, the fitting must be accomplished directly for the whole EXAFS function. The coordination number ($N_{\text{Co-M}}$) and mean deviation ($\sigma_{D_{\text{Co-M}}}$) so obtained preserve the values attained with the previous procedure. Only the Co- M distance results in a slightly higher value. Table II summarizes the results for both fitting procedures.

The Co K -edge EXAFS of $x=5$, $(\text{Fe}_{0.2}\text{Co}_{0.8})_{75}\text{Si}_5\text{B}_{20}$, can be fitted following the same procedure used in $x=0$, neglecting the Si and B contributions. Again, the introduction of B almost does not affect $N_{\text{Co-M}}$ and $\sigma_{D_{\text{Co-M}}}$. We have only appreciated a slight increase of $R_{\text{Co-M}}$. However, the relative increase of $R_{\text{Co-M}}$ from $x=0$ to 5 is the same as the one obtained neglecting the B contribution (see Table II).

In the case of $x=10$ and 15 [$(\text{Fe}_{0.2}\text{Co}_{0.8})_{75}\text{Si}_x\text{B}_{25-x}$], the Si influence over the XANES region of x-ray-absorption spectra indicates that the Co-Si pair contribution cannot be discarded. Therefore, both Co-B and Co-Si pairs have been taken into account to perform the fit. However, the B atom coordination numbers around Co ($N_{\text{Co-B}}$) obtained from the fitting process are close to zero both for $x=10$ and 15 (see Table II).

2. Fe K edge

For the sample $x=0$, $(\text{Fe}_{0.2}\text{Co}_{0.8})_{75}\text{B}_{25}$, expression (6) does not fit the phase of the EXAFS signal $[k\chi^F(k)/A(k)]$. This fact clearly indicates that the B contribution cannot be neglected. The results obtained considering the Fe- M and

TABLE III. Values of structural parameters relative to the neighborhood of Fe atoms for $(\text{Fe}_{0.2}\text{Co}_{0.8})_{75}\text{Si}_x\text{B}_{25-x}$ amorphous samples: coordination numbers N , nearest interatomic distance R , mean deviation of interatomic distance, σ_D , and average interatomic distance $\hat{R} = R + \sigma_D$.

Sample	S	Fe-M				Fe-B				Fe-Si			
		N	R (Å)	σ_D (Å)	\hat{R} (Å)	N	R (Å)	σ_D (Å)	\hat{R} (Å)	N	R (Å)	σ_D (Å)	\hat{R} (Å)
$x=0$	7.11×10^{-3}	10.6 (8)	2.371 (6)	0.23 (2)	2.60 (4)	3.4 (9)	2.17 (4)	0.01 (3)	2.18 (7)				
$x=5$	8.0×10^{-3}	10.5 (9)	2.366 (6)	0.24 (2)	2.61 (4)	2.9 (9)	2.18 (4)	0.00 (3)	2.18 (7)				
	3.47×10^{-3}	10.3 (7)	2.367 (4)	0.24 (2)	2.61 (2)	2.9 (7)	2.16 (3)	0.00 (3)	2.16 (6)	0.9 (5)	2.68 (4)	0.00 (5)	2.68 (9)
$x=10$	4.37×10^{-3}	9.9 (7)	2.365 (5)	0.32 (2)	2.68 (3)	2.6 (8)	2.12 (4)	0.02 (5)	2.14 (9)	1.8 (4)	2.67 (4)	0.00 (3)	2.67 (7)
$x=15$	7.49×10^{-3}	8.7 (6)	2.349 (7)	0.37 (3)	2.72 (4)	2.5 (10)	2.14 (6)	0.01 (6)	2.15 (9)	2.9 (3)	2.67 (4)	0.01 (5)	2.68 (9)

Fe-B contributions in the fitting of the sample $x=0$ are presented in Table III. In order to fit the EXAFS spectra of the samples with increasing Si concentration, we have used the qualitative information obtained from XANES. We deduced previously by XANES that the location of Si as nearest neighbor of Fe should happen very scarcely, and so we can assume that only M and B atoms are located in the nearest neighborhood of Fe atoms. In this way, the EXAFS spectrum of $x=5$ is fitted rather well with a smaller B coordination number ($N_{\text{Fe-B}}$) than in $x=0$, as can be expected from the stoichiometric composition $[(\text{Fe}_{0.2}\text{Co}_{0.8})_{75}\text{Si}_x\text{B}_{25-x}]$ (see Table III). However, the use of only these two contributions $\chi_{\text{Fe-M}}$ and $\chi_{\text{Fe-B}}$ to fit the EXAFS spectra of $x=10$ and 15 does not yield any reliable results. In these samples it becomes clear that we have to take into account the Si contribution in the first coordination shell.

The introduction of the Si atom around Fe at a distance similar to that found for the Co atom ($R_{\text{Fe-Si}} \approx 2.25$ Å) does not fit properly the spectra. This clearly indicates that the Si atom is not placed as a touching sphere to the Fe one in a model of hard spheres. Allowing the Fe-Si distance to vary inside the limits of the first coordination shell (2–3 Å), the Si atom places at 2.67 Å from the Fe atom in $x=10$ and 15 (see Table III). No reliable fit can be obtained neglecting the Fe-B contribution, in agreement with the XANES results.

The introduction of the Si contribution for the sample $x=5$ improves the fit, and the results are very similar to those already obtained neglecting this contribution (see Table III).

V. DISCUSSION

A. Topological short-range order

The experimental EXAFS spectra $\chi(k)$ of the Fe K edge [see Fig. 3(a)] show (marked with an arrow) the appearance of a shoulder at around 4 \AA^{-1} , very clear for $x=15$, which grows gradually with the increase of the Si content. Such a feature can be reproduced performing the inverse Fourier transform of $\Phi(R)$, in a range $1.4 < R < 5.1$ Å that includes the following bumps of the Fourier transform of $\chi(k)$ for $x=15$. So it is evidence of the existence of a longer short-range order involving more coordination shells than the first one.

The results obtained from Mössbauer spectroscopy in $(\text{Fe-Co})_{75}(\text{Si-B})$ (Ref. 12) support the idea about the enhancement of the short-range order in $(\text{Fe}_{20}\text{Co}_{80})_{75}\text{Si}_x\text{B}_{25-x}$ when the Si concentration increases. The standard deviation $\Delta\sigma$ of the hyperfine field distribution (HFD) proved to be a

suitable parameter to evaluate SRO changes in amorphous alloys involving Fe. It was observed that though the main influence over the HFD comes from the Fe/Co relative concentration in $(\text{Fe-Co})_{75}(\text{Si-B})$, the increase of Si content at the expense of B yields a reduction of $\Delta\sigma$ of the HFD without affecting the shape of the HFD. This result together with the dependence of the magnetic hyperfine field and isomer shift on the metal and metalloid concentrations suggests a large SRO increase in the Co-rich side of the system $(\text{Fe-Co})_{75}(\text{Si-B})$ which is strongly affected by changes of the Si/B relative concentration.¹²

Table III shows that the mean deviation of the Fe- M pair distance ($\sigma_{D_{\text{Fe-M}}}$) increases notably with Si concentration, specially for $x=15$. In this case $\sigma_{D_{\text{Fe-M}}}$ becomes much higher than for the other samples and also than those results found by other authors.^{15,17,18,27} If σ_D is understood as a measure of the Fe- M disorder, the previous result stands in contradiction with the longer-range-order increase deduced from the raw EXAFS spectrum of $x=15$ and the Mössbauer results. Moreover, Table III presents a value of $R_{\text{Fe-M}} = 2.35$ Å for $x=15$ that is shorter than the Fe- M interatomic distances obtained in the other samples, and the total metalloid coordination number around Fe is quite high ($N_{\text{Fe-Si}} + N_{\text{Fe-B}} \cong 5.5$) (see Table III).

In the previous paragraph, we have taken σ_D as a measure of the disorder. However, the increase of $\sigma_{D_{\text{Fe-M}}}$ can be regarded as a consequence of a splitting of the Fe- M distances in the first coordination shell, like in a bcc structure. This effect would cause the mean deviation of distances (σ_D) to increase. Table IV shows the values of the structural parameters obtained for $x=15$ by considering the splitting of the Fe- M contribution of the first shell. So the theoretical EXAFS function becomes a linear combination of four EXAFS signals, two $\chi_{\text{Fe-M}}$ plus $\chi_{\text{Fe-B}}$ and $\chi_{\text{Fe-Si}}$. The results shown in Table IV ($R_{\text{Fe-M}} = 2.36$ Å and $N_{\text{Fe-Si}} + N_{\text{Fe-B}} \cong 4$) are more consistent with those obtained for the rest of the samples than the previous one for $x=15$ presented in Table III.

The splitting of the Fe environment on two different “subshells” suggests the existence of a structure similar to a bcc one. In fact, the relation between the two subshells is 1:1.19, very similar to that found in bcc Fe.

In addition, a further indication of the order increase lies in the fact that it is possible to reproduce the raw data spectrum of $x=15$ considering two additional M contributions at 3.37 and 4.11 Å (see Fig. 8). So the shoulder in $\chi(k)$ can be

TABLE IV. Structural parameters obtained assuming a linear combination of four EXAFS signals two $\chi_{\text{Fe-M}}$ plus $\chi_{\text{Fe-B}}$ and $\chi_{\text{Fe-Si}}$ in $(\text{Fe}_{0.2}\text{Co}_{0.8})_{75}\text{Si}_{15}\text{B}_{10}$.

Sample	S	Fe-M				Fe-B				Fe-Si			
		N	R (Å)	σ_D (Å)	\hat{R} (Å)	N	R (Å)	σ_D (Å)	\hat{R} (Å)	N	R (Å)	σ_D (Å)	\hat{R} (Å)
$x=15$	1.57×10^{-3}	7.1 (6)	2.361 (6)	0.25 (3)									
					2.71 (4)	2.2 (7)	2.14 (4)	0.00 (4)	2.14 (8)	1.8 (6)	2.65 (3)	0.09 (5)	2.74 (8)
		2.9 (7)	2.82 (1)	0.13 (3)									

unambiguously related to an atomic order extending to several atomic shells (up to ≈ 5 Å). We suggest that the appearance of such a shoulder in a given spectrum should be taken as an indication of such a degree of order.

B. Chemical short-range order

The most outstanding feature found by both EXAFS and XANES analysis in $(\text{Fe}_{20}\text{Co}_{80})_{75}\text{Si}_x\text{B}_{25-x}$ is the existence of a strong chemical short-range order (CSRO) which yields B to place preferentially near Fe and Si close to Co. This chemical affinity is deduced by the XANES qualitative study as well as by the quantitative EXAFS study. Taking into account that the metalloid atoms avoid direct contact and are exclusively bonded to metal atoms,²⁸⁻³⁰ it becomes clear that the chemical affinities must induce great atomic rearrangements when both the Si and B concentrations are comparable. Although EXAFS analysis does not allow one to distinguish between Fe and Co as backscatterers, metal rearrangements must also occur in order to conform the required bonding conditions of the metalloids.

Figure 9 shows the dependence on Si concentration (x) of the first neighbor distances Fe-M and Co-M ($R_{\text{Fe-M}}$ and $R_{\text{Co-M}}$). The latter increases monotonically with x , while $R_{\text{Fe-M}}$ decreases slightly when x increases. This behavior could be due to the preferred location of the Si atom as a nearest neighbor of the Co one, but not of the Fe atoms. In this sense, the $R_{\text{Co-M}}$ increase, when increasing the Si content, could be explained by the larger Si atomic size with respect to the B one. On the other hand, when increasing the Si content $R_{\text{Fe-M}}$ decreases slightly. This suggests that the Si atom does not substitute to the B one as a nearest neighbor of

the Fe atom. The Si atom is located at a distance of ≈ 2.67 Å around Fe, which indicates that the Si atom is like a “second” neighbor inside the first coordination shell.

The value of the Co-Si pair distance (see Table II) ($R_{\text{Co-Si}} \approx 2.25$ Å) is close to the sum of covalent radii as is indeed the case for the Fe-B pair distance ($R_{\text{Fe-B}} \approx 2.15$ Å) (see Tables III and IV). These results are very similar to those found in other metallic glasses.^{31,32} This fact indicates the covalent character of the Co-Si and Fe-B bonds.

The $M-M$ average distance R_{M-M} increases with increasing the Si content (see Tables II–IV). The values found, between 2.58 and 2.71 Å, are similar to those found in the literature from EXAFS spectroscopy, $\text{Co}_{78}\text{B}_{22}$ (Ref. 33) and $\text{Co}_{78}\text{B}_{22}$ (Ref. 32) ($R_{\text{Co-Co}} = 2.57$ Å), and from diffraction techniques, $\text{Fe}_{82}\text{P}_{18}$ (Ref. 34), $\text{Fe}_{75}\text{P}_{25}$ (Ref. 35) ($R_{\text{Fe-Fe}} = 2.61$ Å), $\text{Fe}_{80}\text{B}_{20}$ (Ref. 36) ($R_{\text{Fe-Fe}} = 2.57$ Å), and $\text{Fe}_{75}\text{B}_{25}$ (Ref. 37) ($R_{\text{Fe-Fe}} = 2.60$ Å).

The coordination number of metalloids B and Si around M obtained from the quantitative EXAFS analysis also agrees with the general trends of the CSRO advanced from the qualitative analysis of XANES. So Fig. 10 shows that the coordination number of B around Fe, though decreasing when the B concentration does, remains around values ($N_{\text{Fe-B}} \approx 2.2$) greater than the coordination number of B around Co in the B-richest sample. When the B concentration begins to decrease (increase of x), the contribution from Co-B pairs can be completely neglected in the EXAFS of the Co K edge.

The Si contribution is not clearly observed in the XANES region of the Fe edge as it is in the Co one, although for $x=15$, the coordination number of Si around Fe,

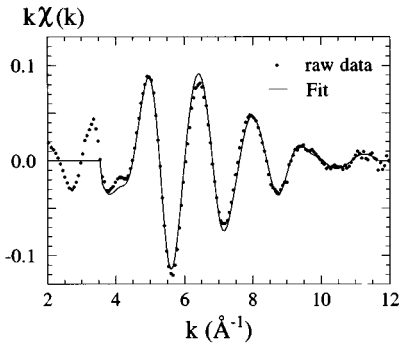


FIG. 8. Raw EXAFS spectrum of $x=15$ compared with the fit of the inverse Fourier transform of $\Phi(R)$ performed in the range $1.4 < R < 5.1$ Å. The fit was performed using the Fe-M contributions corresponding to the first coordination shell (Table IV) plus two other Fe-M contributions (one at 3.37 Å and another at 4.11 Å).

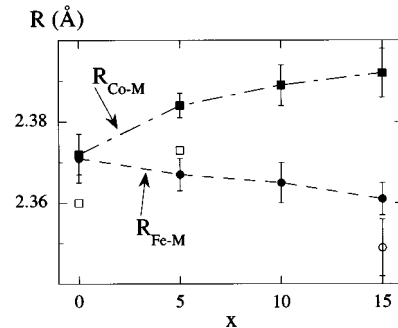


FIG. 9. Dependence of $M-M$ nearest-neighbor distance as a function of Si concentration x in $(\text{Fe}_{0.2}\text{Co}_{0.8})_{75}\text{Si}_x\text{B}_{25-x}$ amorphous samples. The values of $R_{\text{Co-M}}$ are from Table II [\square , considering only a Co-M contribution; \blacksquare , considering Co-M and Co-metalloid (Si or B) contributions]. The values of $R_{\text{Fe-M}}$ are from Tables III and IV (for $x=15$, \bullet , from Table III; \circ , from Table IV).

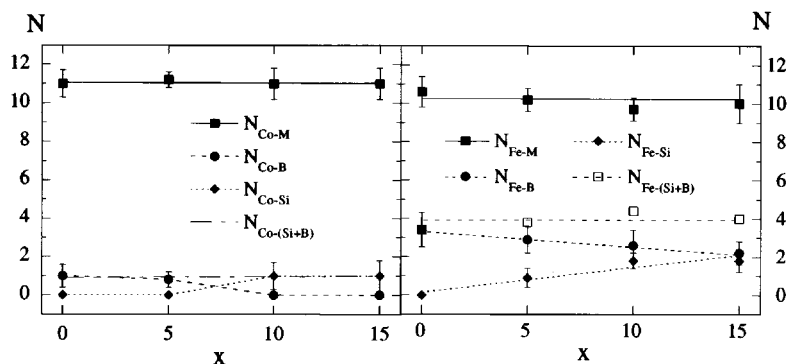


FIG. 10. Dependence of coordination numbers on Si concentration x corresponding to the different atomic pairs in $(\text{Fe}_{0.2}\text{Co}_{0.8})_{75}\text{Si}_x\text{B}_{25-x}$ amorphous samples. The values of coordination numbers around Co are from Table II. The values of coordination numbers around Fe are taken from Table III ($x=0,5,10$) and from Table IV ($x=15$).

$N_{\text{Fe-Si}} \cong 1.8(6)$, is of the order or even higher than that found in the Co neighborhood, $N_{\text{Co-Si}} \cong 1.1(10)$. However, the Si atom is placed at 2.65 \AA from the Fe one, while it is located at a covalence distance $\approx 2.25 \text{ \AA}$ around the Co atom. This can be the reason that underlies the minor influence of Si over the XANES region of the Fe K edge.

Figure 10 also shows that the overall coordination number of Si and B in the first coordination shell both around Fe and Co remains roughly constant within the fitting error ($N_{\text{Fe-Si}} + N_{\text{Fe-B}} \cong 4$, $N_{\text{Co-Si}} + N_{\text{Co-B}} \cong 1$). The coordination number of metals, M , both around Fe and Co, in Fig. 10, lies between 10 and 11. So all of them are the same within the fitting procedure errors and no trend of change is observed with the Si concentration increase. This behavior is expected, taking into account that the total concentration of metal atoms, Fe plus Co, is the same in the four studied samples.

VI. CONCLUSIONS

X-ray-absorption spectroscopy has proved to be a powerful tool to obtain qualitative and quantitative data about the short-range structure in quaternary alloys Fe-Co-Si-B.

The XANES of Fe and Co K edges clearly indicates the existence of a large chemical short-range order with preferential coordination of Fe-B and Co-Si pairs.

The quantitative results from EXAFS agree with the previous conclusion about the CSRO. Thus the Co-Si and Fe-B

pair distances are close to the sum of the covalent radii, indicating the covalent character of these bonds. Although the number of Si atoms located in the first coordination shell of Fe is similar to that found in the Co edge, the Si atoms do not place at a covalent distance of the Fe one. This means that when increasing the Si content, the Si atom does not enter the place of the B one in the structure of $(\text{Fe}_{20}\text{Co}_{80})_{75}\text{Si}_x\text{B}_{25-x}$ alloys.

The increase of the mean deviation of Fe- M pair distances, σ_D , with increasing the Si content, can be understood as due to a topological short-range-order increase of the first coordination shell. The strong chemical affinity of Si with Co results in the M atoms around Fe splitting into two “subshells.”

The shoulder that appears at around 4 \AA^{-1} in the Fe K edge when the Si concentration increases has been related to the existence of a longer-range order than that concerning the first coordination shell.

ACKNOWLEDGMENTS

We thank the Daresbury Laboratory for Synchrotron measurement facilities. We also thank to P.U.L.S. Group at Frascati Laboratory for providing us EXAFS programs. This work has been partially supported by UPV/EHU under Project No. UPV 224.310-EA 056/93. One of the authors (I.O.) thanks to Basque Government for financial support.

¹F. E. Luborsky, in *Ferromagnetic Materials*, Vol. 1, edited by E. P. Wohlfarth (North-Holland, Amsterdam, 1980), Chap. 1.

²O. V. Nielsen, A. Hernando, V. Madurga, and J. M. Gonzalez, *J. Magn. Magn. Mater.* **46**, 341 (1985).

³V. Madurga, M. Vazquez, A. Hernando, and O. V. Nielsen, *Solid State Commun.* **52**, 701 (1984).

⁴J. M. Barandiarán, A. Hernando, V. Madurga, O. V. Nielsen, M. Vazquez, and M. Vazquez-Lopez, *Phys. Rev. B* **35**, 5066 (1987).

⁵H. Fujimori, H. Morita, Y. Obi, and S. Ohita, in *Amorphous Magnetism*, edited by R. A. Levy and R. Hasegawa (Plenum, New York, 1977), Vol. 2, p. 393.

⁶O. V. Nielsen, *IEEE Trans. Magn.* **MAG-21**, 2008 (1985).

⁷R. C. O’Handley, in *Amorphous Magnetism*, edited by R. A. Levy and R. Hasegawa (Plenum, New York, 1977), Vol. 2, p. 379.

⁸A. Hernando, V. Madurga, J. M. Barandiarán, and O. V. Nielsen, *Solid State Commun.* **54**, 1059 (1985).

⁹J. M. Barandiarán, M. L. Fdez-Gubieda, J. Gutierrez, F. Plazaola,

and O. V. Nielsen, *J. Magn. Magn. Mater.* **83**, 334 (1990).

¹⁰T. Kamatsu, S. Sato, and K. Matusita, *Acta Metall.* **34**, 1891 (1986).

¹¹M. L. Fernández-Gubieda, J. M. Barandiarán, F. Plazaola, A. Hernando, and S. Mobilio, *J. Non-Cryst. Solids* **151**, 51 (1992).

¹²F. Plazaola, I. Orue, M. L. Fernández-Gubieda, and J. M. Barandiarán, *J. Appl. Phys.* **77**, 3338 (1995).

¹³H. H. Liebermann and C. D. Graham, *IEEE Trans. Magn.* **MAG-12**, 921 (1976).

¹⁴B. Lengeler and P. Eisenberger, *Phys. Rev. B* **21**, 4507 (1980).

¹⁵E. D. Crozier, J. J. Rehr, and R. Ingalls in *X-Ray Absorption: Principles, Applications and Techniques of EXAFS, SEXAFS and XANES*, edited by D. C. Koningsberger and R. Prins (Wiley, New York, 1988), Chap. 9.

¹⁶P. Eisenberger and G. S. Brown, *Solid State Commun.* **29**, 481 (1979).

¹⁷M. De Crescenzi, A. Balzarotti, F. Comin, L. Incoccia, S. Mo-

- bilio, and N. Motta, *Solid State Commun.* **37**, 921 (1981).
- ¹⁸P. Lagarde, J. Rivory, and G. Vlaic, *J. Non-Cryst. Solids* **57**, 275 (1983).
- ¹⁹J. Mustre de Leon, J. J. Rehr, R. C. Albers, and S. I. Zabinsky, *Phys. Rev. B* **44**, 4146 (1991).
- ²⁰A. G. Mckale, B. W. Veal, A. P. Paulikas, S. K. Chan, and G. S. Knapp, *J. Am. Chem. Soc.* **110**, 3763 (1988).
- ²¹M. L. Fdez-Gubieda, I. Orue, F. Plazaola, and J. M. Barandiaran, *Physica B* **208&209**, 365 (1995).
- ²²*Pearson's Handbook of Crystallographic Data for Intermetallic Phases*, edited by P. Villars and L. D. Calvert (ASM, Metals Park, Ohio, 1985).
- ²³S. Pascarelli, F. Boscherini, S. Mobilio, A. R. Zanatta, F. C. Marques, and I. Chambouleyron, *Phys. Rev. B* **46**, 6718 (1992).
- ²⁴P. Kizler, *Phys. Rev. Lett.* **67**, 3555 (1991).
- ²⁵P. Kizler, *Phys. Rev. B* **47**, 5660 (1993).
- ²⁶P. J. Durham, in *X-Ray Absorption: Principles, Applications, Techniques of EXAFS, SEXAFS and XANES*, edited by D. C. Koningsberger and R. Prins (Wiley, New York, 1988), Chap. 2.
- ²⁷S. Mobilio and L. Incoccia, *Nuovo Cimento* **3**, 846 (1984).
- ²⁸J. D. Bernal, *Nature (London)* **185**, 68 (1960).
- ²⁹D. E. Polk, *Ser. Metall.* **4**, 117 (1970).
- ³⁰J. Wong and H. H. Liebermann, *Phys. Rev. B* **29**, 651 (1984).
- ³¹S. J. Gurman, *J. Mater. Sci.* **17**, 1541 (1982).
- ³²E. Nold, P. Lamperter, H. Olbrich, G. Rainer-Halbach, and S. Steeb, *Z. Naturforsch A* **36**, 1032 (1981).
- ³³J. M. Dubois, G. Le Caer, P. Chieux, and J. Goulon, *Nucl. Instrum. Methods* **199**, 315 (1982).
- ³⁴Y. Waseda and H. S. Chen, *Phys. Status Solidi A* **49**, 387 (1978).
- ³⁵Y. Waseda, H. Okazaki, and T. Masumoto, in *The Structure of Non-Crystalline Materials*, edited by P. H. Gaskell (Taylor & Francis, London, 1977), p. 89.
- ³⁶P. Lamperter, W. Sperl, S. Steeb, and J. Bletry, *Z. Naturforsch. A* **37**, 1223 (1982).
- ³⁷W. Matz, H. Hermann, and N. Mattern, *J. Non-Cryst. Solids* **93**, 217 (1987).